

# A high-rate and stable quasi-solid-state zinc-ion battery with novel 2D layered zinc orthovanadate array

Chao, Dongliang; Zhu, Rose Changrong; Song, Ming; Liang, Pei; Zhang, Xiao; Nguyen, Huy Tiep; Zhao, Haofei; Wang, John; Wang, Rongming; Zhang, Hua; Fan, Hong Jin

2018

Chao, D., Zhu, R. C., Song, M., Liang, P., Zhang, X., Tiep, N. H., ... Fan, H. J. (2018). A high-rate and stable quasi-solid-state zinc-ion battery with novel 2D layered zinc orthovanadate array. *Advanced Materials*, 30(32), 1803181-. doi:10.1002/adma.201803181

<https://hdl.handle.net/10356/92443>

<https://doi.org/10.1002/adma.201803181>

---

This is the peer reviewed version of the following article: Chao, D., Zhu, R. C., Song, M., Liang, P., Zhang, X., Nguyen, H. T., ... Fan, H. J. (2018). A high-rate and stable quasi-solid-state zinc-ion battery with novel 2D layered zinc orthovanadate array. *Advanced Materials*, 30(32), 1803181-, which has been published in final form at <http://dx.doi.org/10.1002/adma.201803181>. This article may be used for non-commercial purposes in accordance with Wiley Terms and Conditions for Use of Self-Archived Versions.

# Advanced Materials

## High-Rate and Stable Quasi-Solid-State Zinc-Ion Battery with Novel 2D Layered Zinc Orthovanadate Array --Manuscript Draft--

<b>Manuscript Number:</b>	
<b>Full Title:</b>	High-Rate and Stable Quasi-Solid-State Zinc-Ion Battery with Novel 2D Layered Zinc Orthovanadate Array
<b>Article Type:</b>	Communication
<b>Section/Category:</b>	
<b>Keywords:</b>	Zinc ion battery; Quasi-solid-state; Layered zinc orthovanadate; Flexible electrode; Zinc array.
<b>Corresponding Author:</b>	Hong Jin Fan Nanyang Technological University Singapore, SINGAPORE
<b>Additional Information:</b>	
<b>Question</b>	<b>Response</b>
Please submit a plain text version of your cover letter here.  <b>If you are submitting a revision of your manuscript, please do not overwrite your original cover letter. There is an opportunity for you to provide your responses to the reviewers later; please do not add them here.</b>	Dear Dr. Esther Levy,  Thank you for giving us the opportunity to resubmit our manuscript (adma.201802147). We have revised it according to your and the reviewers' comments. Repeating sentences have been reworded. Reviewers #1 and 3 are quite positive, and Reviewer #2 questions the novelty, which we can defense. We have addressed all the comments by all three referees. A point to point response is provided separately. I would appreciate if you could reconsider our revised manuscript favorably and avoid the potential conflict of interest with Reviewer #2. This manuscript is very timely given the current hotspot of Zn-ion batteries. In fact, we have submitted an Invited Review to Adv Funct Mater (adfm.201802564) which is currently under minor revision.  ----Major novelty of our paper---- <ul style="list-style-type: none"><li>• Three First: For the 1st time, a novel 2D layered zinc orthovanadate array is synthesized and used as cathode material. The first demonstration of intercalation pseudocapacitance in Zn-ion batteries, especially quasi-solid-state ZIBs. And the 1st report on quasi-solid-state ZIB.</li><li>•Metallic Zn nanoflake array on 3D porous conductive support to replace conventional compact Zn foil anode, which significantly suppresses Zn dendrite growth.</li><li>•We demonstrate a high depth of discharge of ca. 100% for cathode and 66% for anode. In contrast, recent reported ZIBs based on Zn foil anode have very low (&lt; 15%) depth of discharge in the anode because of large amount of non-active Zn materials.</li></ul> ----Justification for resubmission---- <p>Referees #1 and 3 suggest minor revisions. The main concern of Referee #2 is the novelty of our cathode part Zn<sub>2</sub>(OH)VO<sub>4</sub> array. He said there already 7 papers about V-based cathode materials. But the Zn<sub>2</sub>(OH)VO<sub>4</sub> (ZOV) reported herein is a novel 2D layered zinc orthovanadate, which is synthesized for the first time and used as metal ions storage electrode in batteries field. This new cathode also gives new Zn ion storage mechanism: In previous reports of ZIBs, most of the V-based cathode materials are phase-change type, so the rate and cycling performances are all mediocre. The open framework of ZOV shows expanded interlayer spacing (0.73 nm versus 0.57 nm for V<sub>2</sub>O<sub>5</sub> and VS<sub>2</sub>, and 0.58 nm for VO<sub>2</sub>), which is perfect for the 2D (b–c plane) fast ion transport.</p> <p>As a result, we also demonstrate higher performance than before. 89 % capacity retention after 2000 cycles at 20 C, and highest ever energy and power densities (115 Wh kg<sup>-1</sup> and 5100 W kg<sup>-1</sup>, based on mass of both cathode, anode, and current</p>

	collectors).  Sincerely,  Hong Jin Fan School of Physical and Mathematical Sciences Nanyang Technological University, Singapore 21 Nanyang Link, Singapore 637371 E-mail: fanhj@ntu.edu.sg
Do you or any of your co-authors have a conflict of interest to declare?	No. The authors declare no conflict of interest.
<b>Corresponding Author Secondary Information:</b>	
<b>Corresponding Author's Institution:</b>	Nanyang Technological University
<b>Corresponding Author's Secondary Institution:</b>	
<b>First Author:</b>	Dongliang Chao
<b>First Author Secondary Information:</b>	
<b>Order of Authors:</b>	Dongliang Chao
	Changrong Rose Zhu
	Ming Song
	Pei Liang
	Xiao Zhang
	Nguyen Huy Tiep
	Hua Zhang
	Hong Jin Fan
<b>Order of Authors Secondary Information:</b>	
<b>Abstract:</b>	Zinc-ion batteries are under current research focus because of their uniqueness in low cost and high safety. However, it is still desirable to improve the rate performance by improving the Zn <sup>2+</sup> (de)intercalation kinetics and long-cycle stability by eliminating the dendrite formation problem. Herein, we construct the first paradigm of a high-rate and ultra-stable flexible quasi-solid-state zinc ion battery from a novel 2D ultrathin layered zinc orthovanadate array cathode, a conductive porous graphene foam supported Zn array anode, and gel electrolyte. The nanoarray structure for both electrodes assures the high rate capability and alleviates the dendrite growth. The flexible Zn-ion battery has a depth of discharge of ca. 100% for the cathode and 66% for the anode, and delivers an impressive high-rate of 50C (discharge in 60s), long-term durability of 2,000 cycles at 20C, and unprecedented energy density ~115 Wh kg <sup>-1</sup> , together with a peak power density ~5.1 KW kg <sup>-1</sup> (calculation includes masses of cathode, anode and current collectors). First principles calculations and quantitative kinetics analysis show that, the high-rate and stable properties are correlated with the 2D fast ion migration pathways and the introduced intercalation pseudocapacitance.

1 **High-Rate and Stable Quasi-Solid-State Zinc-Ion Battery with Novel 2D**  
2  
3 **Layered Zinc Orthovanadate Array**  
4  
5

6  
7 *By Dongliang Chao, Changrong (Rose) Zhu, Ming Song, Pei Liang\* , Xiao Zhang, Nguyen Huy*  
8 *Tiep, Haoifei Zhao, John Wang, Rongming Wang, Hua Zhang and Hong Jin Fan\**  
9

10  
11  
12 -----  
13  
14 Dr. D. L. Chao, Dr. C. R. Zhu, Dr. M. Song, N. H. Tiep, Prof. H. J. Fan\*  
15 School of Physical and Mathematical Sciences  
16 Nanyang Technological University, 637371, Singapore  
17 Email: [fanhj@ntu.edu.sg](mailto:fanhj@ntu.edu.sg)  
18  
19

20  
21 Dr. M. Song  
22 School of Chemistry and Chemical Engineering  
23 Xuzhou University of Technology, 221018, P. R. China  
24  
25

26  
27 Prof. P. Liang\*  
28 College of Optical and Electronic Technology  
29 China Jiliang University, Hangzhou 310038, P. R. China  
30 Email: [plianghust@126.com](mailto:plianghust@126.com)  
31  
32

33  
34 X. Zhang, Prof. H. Zhang  
35 School of Materials Science and Engineering  
36 Nanyang Technological University, 639798, Singapore  
37  
38

39 Dr. H. F. Zhao, Prof. R. M. Wang,  
40 Beijing Key Laboratory for Magneto-Photoelectrical Composite and Interface Science,  
41 School of Mathematics and Physics,  
42 University of Science and Technology, Beijing, 100083, P. R. China  
43  
44  
45

46 Dr. C. R. Zhu, Prof. J. Wang,  
47 Department of Material Science and Engineering  
48 National University of Singapore, 117574 Singapore  
49  
50

51  
52 **Keywords:** *Zinc ion battery, Quasi-solid-state, Layered zinc orthovanadate, Flexible electrode,*  
53 *Zinc array*  
54  
55  
56  
57  
58  
59  
60

## Abstracts

Zinc-ion batteries are under current research focus because of their uniqueness in low cost and high safety. However, it is still desirable to improve the rate performance by improving the  $\text{Zn}^{2+}$  (de)intercalation kinetics and long-cycle stability by eliminating the dendrite formation problem. Herein, we construct the first paradigm of a high-rate and ultra-stable flexible quasi-solid-state zinc ion battery from a novel 2D ultrathin layered zinc orthovanadate array cathode, a conductive porous graphene foam supported Zn array anode, and gel electrolyte. The nanoarray structure for both electrodes assures the high rate capability and alleviates the dendrite growth. The flexible Zn-ion battery has a depth of discharge of ca. 100% for the cathode and 66% for the anode, and delivers an impressive high-rate of 50C (discharge in 60s), long-term durability of 2,000 cycles at 20C, and unprecedented energy density  $\sim 115 \text{ Wh kg}^{-1}$ , together with a peak power density  $\sim 5.1 \text{ KW kg}^{-1}$  (calculation includes masses of cathode, anode and current collectors). First principles calculations and quantitative kinetics analysis show that, the high-rate and stable properties are correlated with the 2D fast ion migration pathways and the introduced intercalation pseudocapacitance.

Li-ion batteries have been the dominating commercial power source for portable electronics and has achieved great success in the past decades, the scarce abundance (20 ppm) and increasing higher cost of Li pose challenges for its large-scale application<sup>[1-3]</sup>. Zinc offers significant advantages over lithium in terms of the natural abundance, large-scale distribution, easy processing, and nontoxicity<sup>[4]</sup>. Zinc ion batteries (ZIBs) are promising due to their two-electron redox ( $\text{Zn}^{0/2+}$ ), low cost, high safety, as well as easier to scale up than organic Li-ion batteries<sup>[1, 5]</sup>. One of the issues that that has held back the application of Zn in next-generation batteries lies in its poor cycle life and inferior fast-discharge performance due to the dendrite formation on zinc foil anode<sup>[1]</sup>. Recent reported cathode materials include tunnel-type  $\alpha\text{-MnO}_2$ <sup>[6]</sup>,  $\gamma\text{-MnO}_2$ <sup>[7]</sup>, Prussian blue analogs<sup>[8]</sup>, NASICON structured  $\text{Na}_3\text{V}_2(\text{PO}_4)_3$ <sup>[9]</sup>,  $\text{Na}_3\text{V}_2(\text{PO}_4)_2\text{F}_3$ <sup>[10]</sup>, calix[4]quinone<sup>[11]</sup>, layered-type  $\text{LiV}_3\text{O}_8$ <sup>[12]</sup>,  $\text{Na}_{1.1}\text{V}_3\text{O}_{7.9}$ <sup>[13]</sup>,  $\text{VS}_2$ <sup>[14]</sup>, and metal vanadium oxide bronzes<sup>[5, 15]</sup>. Despite these efforts, the high-rate performance and

1 cycling sustainability are still relatively poor, probably due to reasons such as elements  
2 dissolution, self-aggregation, and phase change incorporated in  $\text{Zn}^{2+}$  uptake. Therefore, novel  
3 intercalation cathodes with tailored nanoarchitecture design are prerequisite, which can both  
4 provide short and fast  $\text{Zn}^{2+}$  migration channels and sustain the structure integrity without  
5 crystallographic phases change for long-time and high-rate cycling.  
6  
7  
8  
9

10 To date, three types of Zn-ion storage mechanisms are being discussed in literature, i.e.  
11 diffusion-controlled faradaic process<sup>[4, 8-12]</sup>, the surface-induced pseudocapacitive faradaic  
12 process, and the nonfaradaic contribution from the electrical double-layer capacity (EDLC)  
13 effect.<sup>[14, 15]</sup> In most cases, the EDLC value ranges between  $10\text{--}50\ \mu\text{F cm}^{-2}$  and is considered  
14 negligible<sup>[16]</sup>. It is difficult to achieve high-rate performance based on the first process due to  
15 the poor mass diffusion of divalent cation  $\text{Zn}^{2+}$  in the bulk lattice. It is expected that the second  
16 process should be able to render fast kinetics that is particularly favorable to  $\text{Na}^+/\text{K}^+/\text{Zn}^{2+}$  ion  
17 batteries with cation sizes larger than  $\text{Li}^+$  <sup>[17, 18, 19]</sup>. Particularly in solid-state battery systems,  
18 the progress on faradic capacitive contribution has been very limited.  
19  
20  
21  
22  
23  
24  
25  
26  
27  
28

29 In order to tackle the above issues and achieve high-rate and stable ZIBs, herein we report  
30 our flexible quasi-solid-state Zn-ion battery (QSS-ZIB) by employing a novel layered zinc  
31 orthovanadate as high-performance cathode and zinc nanoflake array as anode. For the anode  
32 part, we synthesized metallic Zn nanoflakes array on a 3D porous conductive support to replace  
33 conventional compact Zn foil. This, together with the use of newly designed quasi-solid-state  
34 electrolyte instead of aqueous electrolyte, Zn dendrite growth is thoroughly eliminated. In the  
35 zinc orthovanadate array cathode side, we show that the thin and mesoporous morphological  
36 features and the associated fast 2D ion migration pathways facilitate a significant intercalation  
37 pseudocapacitive contribution without crystallographic phase change. This flexible all-array  
38 QSS-ZIB enables high rate capability with long-term cycling performance, and delivers  
39 unprecedented maximum energy and power densities as high as  $\sim 115\ \text{Wh kg}^{-1}$  and  $\sim 5100\ \text{W}$   
40  $\text{kg}^{-1}$ , respectively (on the basis of mass from both cathode, anode, and their current collectors).  
41 Our results may stimulate a paradigm shift of ZIB to new  $\text{Zn}^{2+}$  host materials, 3D zinc metal  
42 electrode and solid-state electrolyte, and also afford deeper understanding of the Zn ion  
43 migration processes in such layered host through intercalation pseudocapacitance. Such safe,  
44  
45  
46  
47  
48  
49  
50  
51  
52  
53  
54  
55  
56  
57  
58  
59  
60  
61  
62  
63  
64  
65

cost-effective, and high-energy/power density ZIB may be a promising candidate for safer power sources than the dominating LIBs.

## Characterization of electrode materials

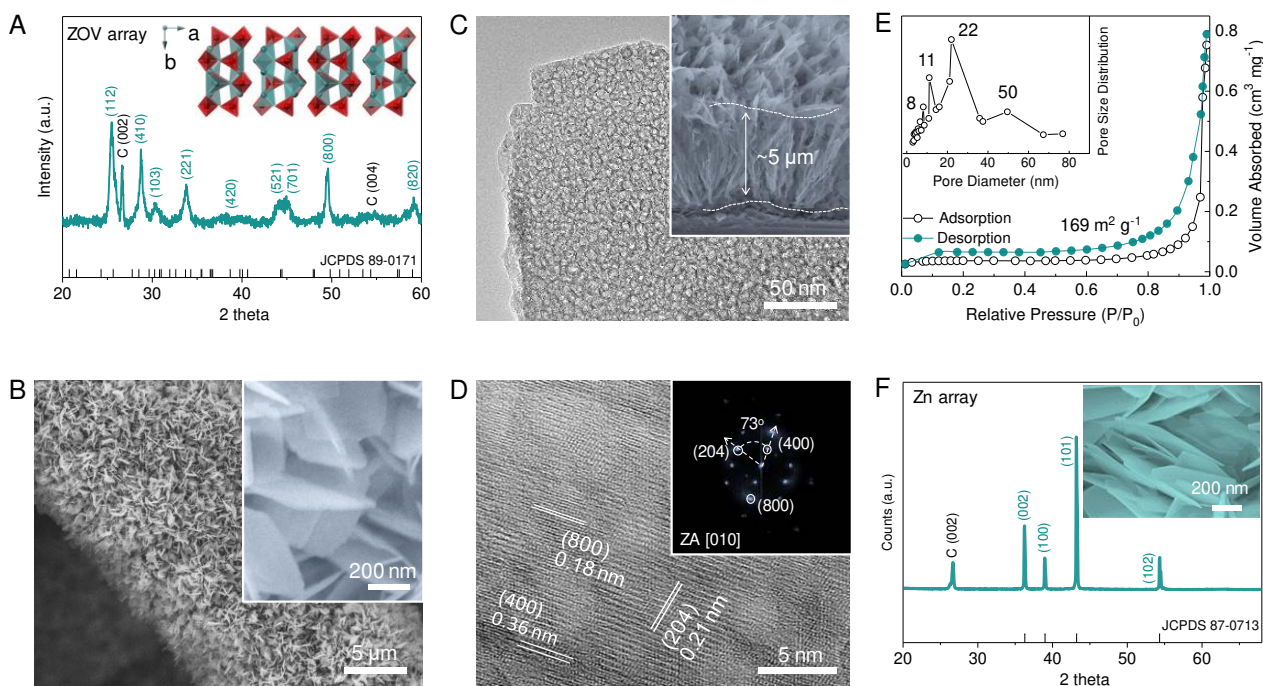


**Figure 1 | Morphology and structure of ZOV array cathode and Zn array anode.** (A) XRD pattern of zinc orthovanadate which can be index to orthorhombic  $Zn_2(OH)VO_4$  (PDF #89–0171). Inset A: illustration of the layered crystal structure. (B) SEM image of the ZOV with a homogeneous nanoflake structure. Inset B: high resolution SEM image. (C) TEM image of ZOV showing porous surface of the array. Inset C: cross-section of the arrays on top of the substrate. (D) High resolution TEM image of ZOV array. Inset D: corresponding fast Fourier transform (FFT) pattern along the [010] zone axis. (E)  $N_2$  adsorption/desorption isotherm of the ZOV array. Inset E: corresponding pore size distribution. (F) XRD spectrum of the electrodeposited Zn array that corresponds to the hexagonal Zn (PDF #87–0713). Inset: SEM image showing the Zn flake-array structure.

The flexible graphene foam (GF) supported ZOV array cathode is synthesized using a hydrothermal route (details in the Experimental Section). As shown in Figure 1A, the X-ray diffraction (XRD) spectrum unveils the characteristic pattern of orthorhombic  $Zn_2(OH)VO_4$  structure (space group  $Pnma$ , with calculated lattice parameters of  $a = 14.68 \text{ \AA}$ ,  $b = 5.98 \text{ \AA}$ ,  $c = 8.87 \text{ \AA}$ , JCPDS #89–0171), except for the (002) and (004) peaks from the carbon substrate (JCPDS #75–1621). The special layered crystal structure of ZOV is shown in inset of Figure



1A. The 3D [Zn(OH)VO<sub>4</sub>] framework is formed with building blocks of tetrahedra [VO<sub>4</sub>] interconnected with octahedral [ZnO<sub>6</sub>] chain and Zn cations that fill the voids with trigonal octahedral and bipyramidal coordination, which further enhances the structural stability of the open framework and expands the interlayer spacing (0.73 nm *versus* 0.57 nm for V<sub>2</sub>O<sub>5</sub> and VS<sub>2</sub>, and 0.58 nm for VO<sub>2</sub>)<sup>[14, 20, 21]</sup> for 2D fast ion transport along the *b*–*c* plane.

The overall morphologies and crystal phases of the as-prepared ZOV array are characterized using scanning electron microscope (SEM), energy-dispersive X-ray (EDX) elemental mapping, and high-resolution transmission electron microscope (HRTEM) images (see data in Figure 1B–D and Figure S1, Supporting Information). In the nanoarchitecture, each lamellar structure is interconnected with each other and thus can facilitate the electrochemical reactions. Noticeably, the ZOV electrode shows a robust mechanical stability and good flexibility (inset in Figure S2A, Supporting Information); It can be bent without any protection, and the film with a high mass loading  $\sim 4.1 \text{ mg cm}^{-2}$  does not peel off during repeated bending. The nanoflakes have typical thickness less than 10 nm (inset in Figure 1B–C and Figure S1, Supporting Information), average lateral width of ca. 400 nm, height ca. 5  $\mu\text{m}$ , and a highly mesoporous structure (5–10 nm, Figure 1C, and Figure S2, Supporting Information). The lateral view of the array in Figure 2D also discovers the single crystalline feature of the array and interplanar spacings of 3.6, 1.8, and 2.1  $\text{\AA}$  for the (400), (800), and (204) planes, respectively, in correlation with the fast Fourier transform pattern along the [010] zone axis. The formation of nanosheets by (010) facets stacking can also be confirmed with extensively exposed channels in *b*–*c* planes. The specific surface area is measured  $\sim 169 \text{ m}^2 \text{ g}^{-1}$  with pores around 8, 10, 22, and 50 nm, indicating a highly mesoporous feature of the arrays. In addition, the metallic zinc array (ca. 20 nm in thickness and ca. 400 nm in width) on GF substrate as the anode is achieved by a facile electrodeposition method (XRD data is shown in Figure 1F).

## Electrochemistry and battery performance



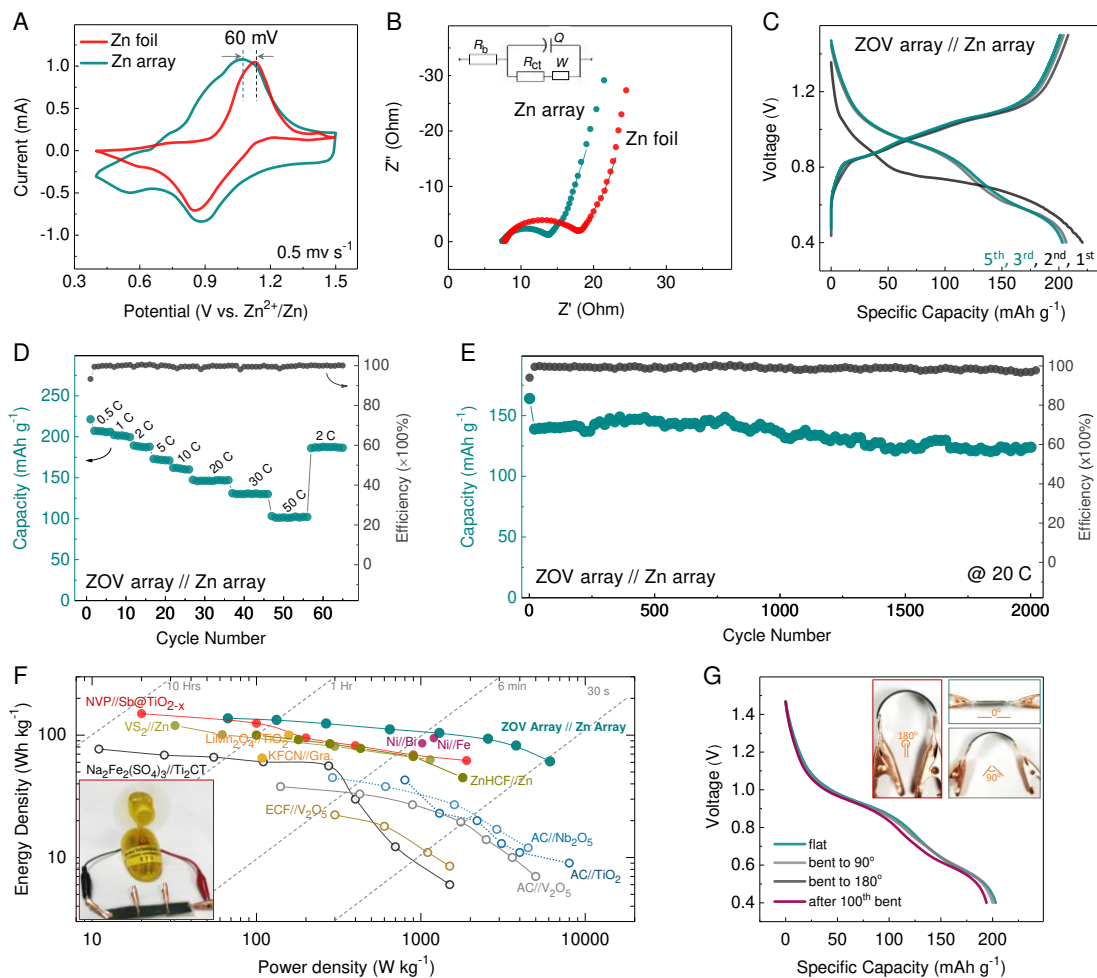


**Figure 2 | Quasi-solid-state ZIB performance with ZOV array as cathode and Zn array as anode.** (A) CV curves comparison after 5 cycles charge/discharge activation at 0.5C of the QSS-ZIBs made of ZOV cathode and Zn array or foil anode (voltage range 0.4 ~ 1.5 V, scan speed  $0.5 \text{ mV s}^{-1}$ ). (B) EIS of the foregoing Zn array and Zn foil electrodes at the fully charged state. An equivalent circuit of  $R_b(Q(R_{ct}W))$  in the inset is used to simulate the resistances, where  $R_b$ ,  $R_{ct}$ ,  $Q$ , and  $W$  are the ohmic resistance of solution and electrodes, the charge transfer resistance, the double layer capacitance, and the Warburg impedance, respectively. (C) Charge-discharge curves of the ZOV array//Zn array device at 0.5C, and (D) rate capability of the cell at varied current densities from 0.5C to 50C. (E) Long-term cycling performance at 20C for 2000 cycles. (F) Ragone plot comparing with other state-of-the-art reported energy storage systems. The calculation includes the mass of active material in both cathode and anode. Inset: Photograph of a small rotation motor (3 V, 0.4 W) connected with fan powered by 3 QSS-ZIBs in series after charging for only 30 seconds. Solid yellow circles are aqueous Li-ion battery of  $\text{LiMn}_2\text{O}_4//\text{TiO}_2$ <sup>[28]</sup>, K-ion battery of  $\text{K}_2\text{Fe}^{\text{II}}[\text{Fe}^{\text{II}}(\text{CN})_6] \cdot 2\text{H}_2\text{O}//\text{Graphite}$ <sup>[29]</sup>; Solid dark yellow circles attribute to aqueous Zn-ion battery of  $\text{VS}_2//\text{Zn}$ <sup>[14]</sup>,  $\text{ZnHCF}//\text{Zn}$ <sup>[8]</sup>; Solid red circles represent Na-ion battery of  $\text{NVP}//\text{Sb}@\text{TiO}_{2-x}$ <sup>[30]</sup>; Solid purple circles are  $\text{Ni}/\text{Fe}$ <sup>[31]</sup>,  $\text{Ni}/\text{Bi}$ <sup>[32]</sup> cells; Yellow empty circles are supercapacitor:  $\text{ECF}//\text{V}_2\text{O}_5$ <sup>[33]</sup>; Black empty circles denote to Na-ion hybrid capacitors:  $\text{AC}//\text{V}_2\text{O}_5$ <sup>[34]</sup>,  $\text{Na}_2\text{Fe}_2(\text{SO}_4)_3//\text{Ti}_2\text{CT}$ <sup>[35]</sup>; Blue empty circles are Li-ion hybrid capacitors:  $\text{AC}//\text{TiO}_2$ <sup>[36]</sup>,  $\text{AC}//\text{Nb}_2\text{O}_5$ <sup>[37]</sup>; (G) The discharge curves of the QSS-ZIB under flat, severe bent status (photographs shown as inset), and after repeated bending for 100 times.

1  
2 To demonstrate its application in Zn ion battery, we assembled flexible quasi-solid-state  
3 full cells using the as-obtained ZOV array as the cathode and Zn array (or Zn foil for  
4 comparison) as the anode. Fumed silica/ZnSO<sub>4</sub> with an ionic conductivity ~8.1 mS cm<sup>-1</sup> at  
5 room temperature (Figure S3, Supporting Information) was used as the electrolyte. It should  
6 be mentioned that all the QSS-ZIBs herein have excessive mass loading of the anode part and  
7 the specific capacity was calculated based on the mass of the ZOV array. And the zinc mass in  
8 QSS-ZIBs with Zn foil is much higher than that assembled with Zn array. As can be seen clearly  
9 from the Cyclic voltammetry (CV) curves in Figure 2A, the QSS-ZIB with Zn array anode  
10 displays larger curve area (higher capacity) and smaller polarization. Electrochemical  
11 impedance spectroscopy (EIS) in Figure 2B shows lower charge-transfer resistance ( $R_{ct}$ ) of the  
12 Zn nanoflake array than the Zn foil ( $R_{ct}$  6.3  $\Omega$  for Zn array *versus* 13.5  $\Omega$  for Zn foil) after  
13 cycles. This also implies a higher surface electron mobility and improved electrochemical  
14 activity when the former is used as anode. Herein we utilize 3D conductive GF substrate  
15 supported Zn array as the anode because of two main advantages over conventional Zn foils:  
16 *First*, the 3D porous GF acts as both a light-weight backbone for the growth of Zn array, and a  
17 continuous current flow channels as well as macroporous agent to alleviate dendrite growth.  
18 Using Zn foil will have the issue of severe growth of a thick inactive surface oxide or hydroxide  
19 layer with low conductivity and reversibility,<sup>[6, 22, 23]</sup> leading to device deterioration especially  
20 in long-term cycles due to the electron blocking (see Figure S4–6, Supporting Information).  
21 *Second*, the short ion diffusion length, high surface area, and more reactive sites features of the  
22 zinc nanoarray structure is favorable for the fast and reversible Zn/Zn<sup>2+</sup> redox kinetics, leading  
23 to high-rate capability. Also, the array structure also diminishes the formation of dendrites and  
24 thus favorable to the enhanced long-term cycling stability.<sup>[19, 23, 24]</sup>

25  
26  
27  
28  
29  
30  
31  
32  
33  
34  
35  
36  
37  
38  
39  
40  
41  
42  
43  
44  
45  
46  
47  
48  
49  
50 From the galvanostatic charge–discharge curves in Figure 2C, one can see that the first Zn<sup>2+</sup>  
51 uptake process initially undergoes a sharp potential drop and then becomes steady. This implies  
52 a relatively large electrochemical polarization that might be due to deactivated surfaces of both  
53 electrodes. The subsequent curves almost overlap, suggesting a stable structure reversibility  
54 and surface state after the activation. A rather high initial coulombic efficiency ~95% is  
55  
56  
57  
58  
59  
60

1 achieved with maintained reversible capacity  $\sim 204 \text{ mAh g}^{-1}$  at 0.5C ( $200 \text{ mA g}^{-1}$  is equivalent  
2 to 1 C), corresponding to an  $\approx 2$  electron redox process. The continuous discharge profiles show  
3 two plateau-like regions located at 1.0–0.7 V and 0.6–0.4 V, which presumably correspond to  
4 the insertion/extraction of  $\text{Zn}^{2+}$  ions from ZOV crystal structure. The result is in  
5 correspondence with the rectangular shape and broaden peaks in the foregoing CV curve, which  
6 are typical features of capacitive charge storage behavior of battery materials (to be discussed  
7 below).

8  
9  
10  
11  
12  
13  
14 The high-rate ability has been regarded as a pivotal indicator for largescale application of  
15 batteries, such as fast recharging of cellphones and electric vehicles, and regenerative braking.  
16 In this regard, the porous thin ZOV nanoarray structure with exposed 2D ion channels is vital  
17 to facilitate ion access and accelerate charge transfer at the electrode/electrolyte interface with  
18 short  $\text{Zn}^{2+}$  and electronic transport path. The high rate performance is evidenced in Figure 2D.  
19 The discharge capacities retain more than  $160 \text{ mAh g}^{-1}$  at 10C and  $101 \text{ mAh g}^{-1}$  at 50C. Finally,  
20 our QSS-ZIB exhibits excellent cycling sustainability even at high rates. The capacity keeps  
21 nearly flat in the first 800 cycles, and a specific capacity of  $125 \text{ mA h g}^{-1}$  can still be maintained  
22 at 20C after 2,000 cycles (ca. 89% of the initial value). In contrast, when aqueous electrolyte  
23 is used, the device shows obvious particle aggregation and the capacity retention is 72% after  
24 only 500 cycles (Figure S6–8, Supporting Information). To the best of our knowledge, this is  
25 the first demonstration of a rechargeable solid-state Zn ion battery with such a long high-rate  
26 lifespan.<sup>[6, 15, 25, 26]</sup> This stability is not accidental, but can be ascribed to the suppressed  
27 chemical dissolution of amphoteric V<sup>[20, 27]</sup> and well preserved structural stability of ZOV by  
28 solid-state electrolyte.

29  
30  
31  
32  
33  
34  
35  
36  
37  
38  
39  
40  
41  
42  
43  
44  
45  
46  
47  
48  
49  
50  
51  
52  
53  
54  
55  
56  
57  
58  
59  
60  
61  
62  
63  
64  
65  
66  
67  
68  
69  
70  
71  
72  
73  
74  
75  
76  
77  
78  
79  
80  
81  
82  
83  
84  
85  
86  
87  
88  
89  
90  
91  
92  
93  
94  
95  
96  
97  
98  
99  
100  
101  
102  
103  
104  
105  
106  
107  
108  
109  
110  
111  
112  
113  
114  
115  
116  
117  
118  
119  
120  
121  
122  
123  
124  
125  
126  
127  
128  
129  
130  
131  
132  
133  
134  
135  
136  
137  
138  
139  
140  
141  
142  
143  
144  
145  
146  
147  
148  
149  
150  
151  
152  
153  
154  
155  
156  
157  
158  
159  
160  
161  
162  
163  
164  
165  
166  
167  
168  
169  
170  
171  
172  
173  
174  
175  
176  
177  
178  
179  
180  
181  
182  
183  
184  
185  
186  
187  
188  
189  
190  
191  
192  
193  
194  
195  
196  
197  
198  
199  
200  
201  
202  
203  
204  
205  
206  
207  
208  
209  
210  
211  
212  
213  
214  
215  
216  
217  
218  
219  
220  
221  
222  
223  
224  
225  
226  
227  
228  
229  
230  
231  
232  
233  
234  
235  
236  
237  
238  
239  
240  
241  
242  
243  
244  
245  
246  
247  
248  
249  
250  
251  
252  
253  
254  
255  
256  
257  
258  
259  
260  
261  
262  
263  
264  
265  
266  
267  
268  
269  
270  
271  
272  
273  
274  
275  
276  
277  
278  
279  
280  
281  
282  
283  
284  
285  
286  
287  
288  
289  
290  
291  
292  
293  
294  
295  
296  
297  
298  
299  
300  
301  
302  
303  
304  
305  
306  
307  
308  
309  
310  
311  
312  
313  
314  
315  
316  
317  
318  
319  
320  
321  
322  
323  
324  
325  
326  
327  
328  
329  
330  
331  
332  
333  
334  
335  
336  
337  
338  
339  
340  
341  
342  
343  
344  
345  
346  
347  
348  
349  
350  
351  
352  
353  
354  
355  
356  
357  
358  
359  
360  
361  
362  
363  
364  
365  
366  
367  
368  
369  
370  
371  
372  
373  
374  
375  
376  
377  
378  
379  
380  
381  
382  
383  
384  
385  
386  
387  
388  
389  
390  
391  
392  
393  
394  
395  
396  
397  
398  
399  
400  
401  
402  
403  
404  
405  
406  
407  
408  
409  
410  
411  
412  
413  
414  
415  
416  
417  
418  
419  
420  
421  
422  
423  
424  
425  
426  
427  
428  
429  
430  
431  
432  
433  
434  
435  
436  
437  
438  
439  
440  
441  
442  
443  
444  
445  
446  
447  
448  
449  
450  
451  
452  
453  
454  
455  
456  
457  
458  
459  
460  
461  
462  
463  
464  
465  
466  
467  
468  
469  
470  
471  
472  
473  
474  
475  
476  
477  
478  
479  
480  
481  
482  
483  
484  
485  
486  
487  
488  
489  
490  
491  
492  
493  
494  
495  
496  
497  
498  
499  
500  
501  
502  
503  
504  
505  
506  
507  
508  
509  
510  
511  
512  
513  
514  
515  
516  
517  
518  
519  
520  
521  
522  
523  
524  
525  
526  
527  
528  
529  
530  
531  
532  
533  
534  
535  
536  
537  
538  
539  
540  
541  
542  
543  
544  
545  
546  
547  
548  
549  
550  
551  
552  
553  
554  
555  
556  
557  
558  
559  
560  
561  
562  
563  
564  
565  
566  
567  
568  
569  
570  
571  
572  
573  
574  
575  
576  
577  
578  
579  
580  
581  
582  
583  
584  
585  
586  
587  
588  
589  
590  
591  
592  
593  
594  
595  
596  
597  
598  
599  
600  
601  
602  
603  
604  
605  
606  
607  
608  
609  
610  
611  
612  
613  
614  
615  
616  
617  
618  
619  
620  
621  
622  
623  
624  
625  
626  
627  
628  
629  
630  
631  
632  
633  
634  
635  
636  
637  
638  
639  
640  
641  
642  
643  
644  
645  
646  
647  
648  
649  
650  
651  
652  
653  
654  
655  
656  
657  
658  
659  
660  
661  
662  
663  
664  
665  
666  
667  
668  
669  
670  
671  
672  
673  
674  
675  
676  
677  
678  
679  
680  
681  
682  
683  
684  
685  
686  
687  
688  
689  
690  
691  
692  
693  
694  
695  
696  
697  
698  
699  
700  
701  
702  
703  
704  
705  
706  
707  
708  
709  
710  
711  
712  
713  
714  
715  
716  
717  
718  
719  
720  
721  
722  
723  
724  
725  
726  
727  
728  
729  
730  
731  
732  
733  
734  
735  
736  
737  
738  
739  
740  
741  
742  
743  
744  
745  
746  
747  
748  
749  
750  
751  
752  
753  
754  
755  
756  
757  
758  
759  
760  
761  
762  
763  
764  
765  
766  
767  
768  
769  
770  
771  
772  
773  
774  
775  
776  
777  
778  
779  
780  
781  
782  
783  
784  
785  
786  
787  
788  
789  
790  
791  
792  
793  
794  
795  
796  
797  
798  
799  
800  
801  
802  
803  
804  
805  
806  
807  
808  
809  
810  
811  
812  
813  
814  
815  
816  
817  
818  
819  
820  
821  
822  
823  
824  
825  
826  
827  
828  
829  
830  
831  
832  
833  
834  
835  
836  
837  
838  
839  
840  
841  
842  
843  
844  
845  
846  
847  
848  
849  
850  
851  
852  
853  
854  
855  
856  
857  
858  
859  
860  
861  
862  
863  
864  
865  
866  
867  
868  
869  
870  
871  
872  
873  
874  
875  
876  
877  
878  
879  
880  
881  
882  
883  
884  
885  
886  
887  
888  
889  
890  
891  
892  
893  
894  
895  
896  
897  
898  
899  
900  
901  
902  
903  
904  
905  
906  
907  
908  
909  
910  
911  
912  
913  
914  
915  
916  
917  
918  
919  
920  
921  
922  
923  
924  
925  
926  
927  
928  
929  
930  
931  
932  
933  
934  
935  
936  
937  
938  
939  
940  
941  
942  
943  
944  
945  
946  
947  
948  
949  
950  
951  
952  
953  
954  
955  
956  
957  
958  
959  
960  
961  
962  
963  
964  
965  
966  
967  
968  
969  
970  
971  
972  
973  
974  
975  
976  
977  
978  
979  
980  
981  
982  
983  
984  
985  
986  
987  
988  
989  
990  
991  
992  
993  
994  
995  
996  
997  
998  
999  
1000

The Ragone plot in Figure 2F compares the array-based ZOV//Zn QSS-ZIB with other reported energy storage devices, such as aqueous supercapacitors, Ni//Fe, Ni//Bi, Li-ion batteries, K-ion batteries, Zn-ion batteries, and organic Li- or Na-ion hybrid capacitors. Our device exhibits a maximum energy density of ca.  $140 \text{ Wh kg}^{-1}$  (with power density  $70 \text{ W kg}^{-1}$ ) and a maximum power density of  $6200 \text{ W kg}^{-1}$  (with energy density  $65 \text{ Wh kg}^{-1}$ ) based on the total active material mass of cathode and anode. More strikingly, the maximum energy density based on the mass of the whole electrode (including current collector) maintains at ca.  $115 \text{ Wh kg}^{-1}$ .

1 kg<sup>-1</sup> thanks to the light-weight GF current collector and freestanding feature (0.6 mg cm<sup>-2</sup>  
2 *versus* ~10 mg cm<sup>-2</sup> for Ti/Zn/stainless steel foils, and ~15 mg cm<sup>-2</sup> for carbon **cloth**). This  
3 value corresponds to at least 200% increase in the energy density compared with traditional  
4 ZIBs with metal foils or carbon cloth supported cathodes and zinc foil incorporated anodes.  
5 Our QSS-ZIB shows a respective depth of discharge of ca. 100% for the ZOV array cathode  
6 and 66% for the zinc array anode, which is superior than the reported ZIBs (49% for quinone  
7 and much lower for other Zn foil based ZIBs)<sup>[1, 2, 5, 11]</sup>. On the basis of a comprehensive  
8 summary, this is so far the best energy/power densities (including cathode, anode, and current  
9 collectors) among reported ZIBs. As summarized in Figure 2F, these characteristics are at least  
10 comparable to and probably slightly better than the best Li<sup>+</sup>/Na<sup>+</sup> ion hybrid capacitors, and  
11 solid-state Li<sup>+</sup>/Na<sup>+</sup> ion batteries reported to date.  
12  
13  
14  
15  
16  
17  
18  
19  
20  
21  
22

23 Additionally, our device can be bent without deteriorating their discharge profiles and  
24 capacities (Figure 2G), and there is no obvious capacity sacrifice (>96% retention) after  
25 repeated 100 times bending. To demonstrate the applications, we show that three QSS-ZIB  
26 cells in series connection, after charging for only 30 sec, can power a rotation motor (3 V, 0.4  
27 W) and fan (inset in Figure 2F). In a nutshell, our all-array QSS-ZIB based on ZOV cathode//Zn  
28 anode exhibits an excellent Zn<sup>2+</sup> storage property with superior high-rate cycling stability, as  
29 well as high energy/power density, and can meet the rapid power change from the grid.  
30  
31  
32  
33  
34  
35  
36  
37  
38  
39

### 40 **Zinc migration mechanism**

41  
42  
43  
44  
45  
46  
47  
48  
49  
50  
51  
52  
53  
54  
55  
56  
57  
58  
59  
60  
61  
62  
63  
64  
65

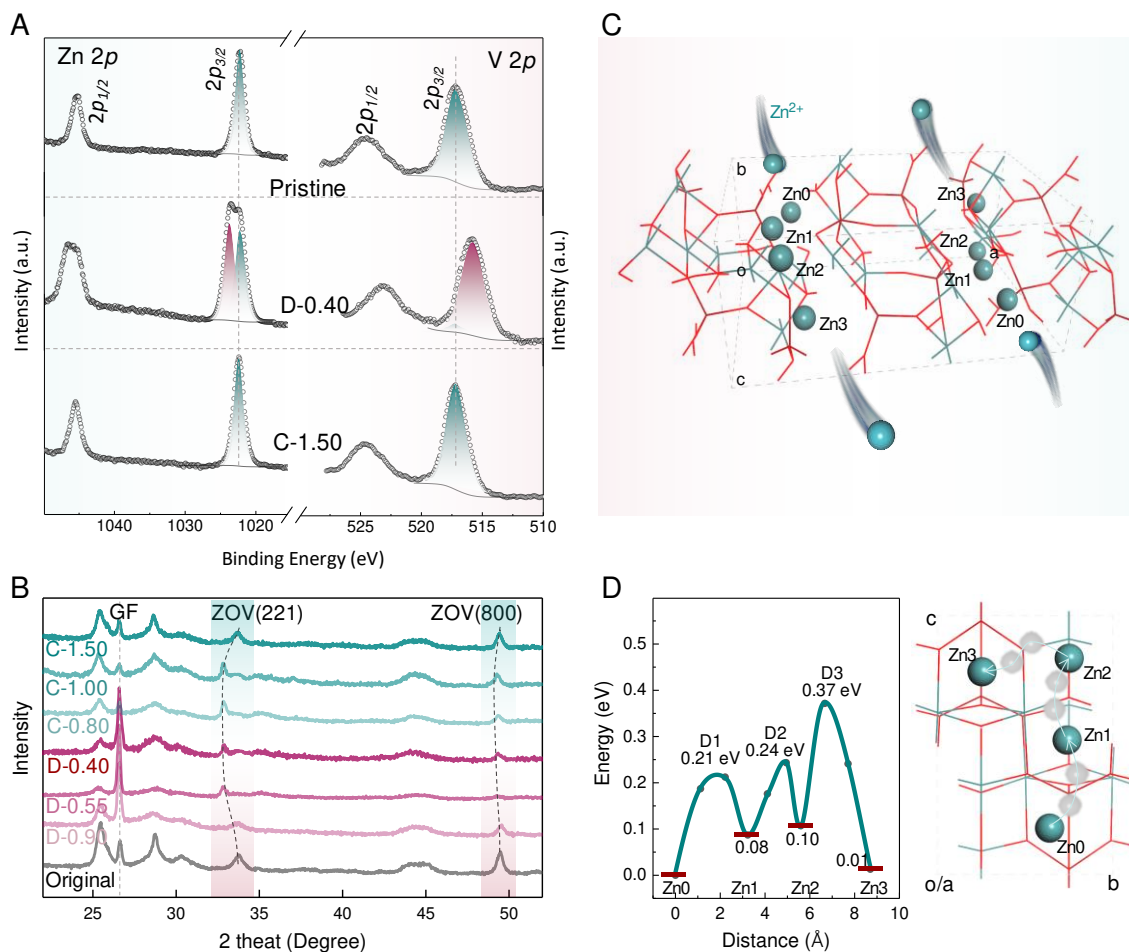


**Figure 3 | Zn<sup>2+</sup> migration in 2D ZOV array cathode.** (A) *Ex-situ* high-resolution XPS spectra of the Zn 2p and V 2p in pristine, fully discharge (D-0.40), and charge (C-1.50) stage. (B) *Ex-situ* XRD patterns as a function of different voltage stages collected during the second galvanostatic discharge–charge profile at 0.5C. (C) Molecular structure evolution from Zn<sub>2</sub>(OH)VO<sub>4</sub> (stick mode) to Zn<sub>3</sub>(OH)VO<sub>4</sub> upon Zn<sup>2+</sup> insertion (green balls) with four different zinc occupation sites denoted with Zn0, Zn1, Zn2, and Zn3. The schematic illustration of zinc shuttles showing the Zn<sup>2+</sup> extraction/insertion 2D paths along exposed b–c planes. (D) First-principle calculation of the in-plane b–c diffusion energy barriers and the corresponding pathways for Zn-ion migration. The arrows indicate optimum diffusion paths.

We use *ex-situ* XPS and XRD to provide more insight about the structural evolution of the 2D ZOV array electrode during charge/discharge cycles. In the Zn 2p region, only one peak of Zn 2p<sub>2/3</sub> component (1022.2 eV) from the original Zn sites in ZOV is observed for the pristine and fully charged (C-1.50) stages. Both this Zn 2p<sub>2/3</sub> peak and the V 2p<sub>2/3</sub> (V<sup>5+</sup> signal at 517.2 eV) recover to their original position after a full charge/discharge cycle, indicating excellent composition reversibility of the ZOV array. After full discharge (D-0.40), one new peak of Zn

1  $2p_{2/3}$  component arises at the higher binding energy of 1023.6 eV, which is due to the ingoing  
2 Zn ions<sup>[5, 26]</sup>. Correspondingly, a red-shift of the V  $2p_{2/3}$  peak to V<sup>3+</sup> component is also  
3 evidently seen<sup>[5, 38]</sup>, which is in accordance with the 2-electron redox reaction shown in the  
4 previous galvanostatic discharge–charge result. Further insight is disclosed by XRD and  
5 Raman investigation (see details in Figure S9, Supporting Information). It can be seen from  
6 Figure 3B that the characteristics (221) and (800) peaks shift to smaller 2 theta angles during  
7 Zn<sup>2+</sup> intercalation and return to their original positions in the subsequent deintercalation. No  
8 new peaks appear. Hence the XPS and XRD data suggest that the intercalation and  
9 deintercalation cycle involves a solid solution reaction without any structure transition.

10  
11  
12  
13  
14  
15  
16  
17  
18  
19 On the basis of the above results, the electrochemical reaction during the Zn<sup>+</sup> ion storage  
20 process of the ZOV array can be described using the equation:  $Zn_2(OH)VO_4 + Zn^{2+} + 2e^- \leftrightarrow$   
21  $Zn_3(OH)VO_4$ . Its local structure evolution after Zn-ion intercalation was estimated based on  
22 density functional theory calculation with GGA–PBE (see details in Method part). Four  
23 different zinc occupation sites denoted with Zn0, Zn1, Zn2, and Zn3 can be found in the  $b$ – $c$   
24 planes in Figure 3C. The fast kinetics of the ZOV array are consistent with the low Zn<sup>2+</sup>  
25 migration energy barriers. Figure 3D shows the calculated in-plane ( $b$ – $c$ ) Zn-ions migration  
26 pathways D1, D2, and D3, where D1 (from the Zn0 site to a neighboring Zn1 site) exhibits the  
27 smallest energy barrier of 0.21 eV. As a comparison, other traditional cathode framework  
28 structures such as LiFePO<sub>4</sub> (0.55 eV for Li<sup>+</sup>), NaFePO<sub>4</sub> (0.32–3.03 eV for Na<sup>+</sup>), Na<sub>2</sub>Fe<sub>2</sub>(SO<sub>4</sub>)<sub>3</sub>  
29 (0.55–1.0 eV for Na<sup>+</sup>) with 1D migration channels, Na<sub>2</sub>FePO<sub>4</sub>F (0.31–0.59 eV for Na<sup>+</sup>), V<sub>2</sub>O<sub>5</sub>  
30 (0.39–1.66 eV for K<sup>+</sup>), TiS<sub>2</sub> (1.16 eV for Mg<sup>2+</sup>), VO<sub>2</sub> (0.5 eV for Al<sup>3+</sup>) with 2D migration  
31 channels, show much higher energy barriers<sup>[39]</sup>. These calculations suggest that the largely  
32 exposed  $b$ – $c$  plane with small thickness, which is parallel to the 2D diffusion paths, is favorable  
33 for fast Zn<sup>2+</sup> migration and high rate energy storage.

### 51 52 **Intercalation pseudocapacitance**

53  
54 After we have confirmed the solid solution reaction mechanism without phase  
55 transformation on (de)intercalation, facile 2D ion diffusion pathways, and the superior fast  
56 charge/discharge, it is reasonable to deduce that an intercalation pseudocapacitive behavior  
57  
58  
59

exist in our QSS-ZIB.<sup>[40]</sup> Here, electrochemical kinetic analysis was carried out to gain further insight into the pseudocapacitive charge storage and diffusion-controlled processes of the all-array based ZOV//Zn QSS-ZIB<sup>[17, 41]</sup>. The degree of capacitive effect can be qualitatively analyzed by the power law relationship between scan rate  $v$  and current  $i$  ( $i = av^b$ , where  $a$  and  $b$  are constants,<sup>[17, 41]</sup>  $b = 0.5$  for a diffusion-controlled process and 1.0 for a capacitor-like process<sup>[42]</sup>). The  $b$  values at anodic and cathodic peaks are 0.95 and 0.89, respectively, indicating a capacity contribution from surface-induced pseudocapacitive behavior (Figure 4A). The CV curves at various scan rates with similar shapes are shown in Figure S10, Supporting Information. The ratio of Zn-ion pseudocapacitive contribution from the total capacity can be quantified by separating the diffusion-controlled and pseudocapacitive current response<sup>[42]</sup> (Figure 4B). Around 78% of the total capacity is found capacitive, even at a relatively slow rate of  $1.0 \text{ mV s}^{-1}$ , which increases with accelerating the scan rate reaching 91% at  $5.0 \text{ mV s}^{-1}$  (Figure 4C). The specific capacity is found much larger than the typical EDLC<sup>[43]</sup>, suggesting that the capacitive current is dominated by an intercalation pseudocapacitive behavior except for the convex peak region. It is likely that the high fraction of capacitive current observed in this QSS-ZIB system stem from the mesoporous and thin-sheet array features of the both electrodes<sup>[44]</sup>. Hence, it is not surprising that our all-array based ZOV//Zn QSS-ZIB leads to a high-rate and stable Zn-ion storage.

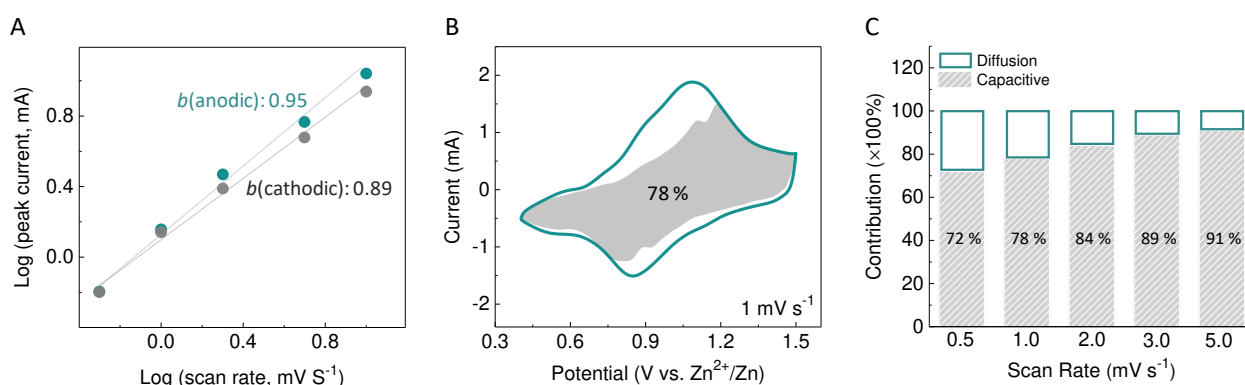


**Figure 4 | Intercalation pseudocapacitive behavior analysis.** (A) Dependence of the peak anodic ( $\sim 1.17 \text{ V}$ ) and cathodic ( $\sim 0.80 \text{ V}$ ) peak currents on the scan rate from  $0.5$  to  $10 \text{ mV s}^{-1}$ . (B) Capacitive contribution (gray part) and diffusion contribution (void part) at  $1.0 \text{ mV s}^{-1}$ . (C) Normalized contribution ratios of capacitive (gray part) capacity at different scan rate.



1 In summary, we report the synthesis of a new 2D layered zinc orthovanadate (ZOV) and  
2 demonstrated its outstanding property as the cathode material in rechargeable zinc-ion battery  
3 (ZIB). The superior  $\text{Zn}^+$  storage performance is a result of the ultrathin mesoporous array  
4 feature with high surface areas and single-crystalline layered structural property with short 2D  
5 fast ion migration pathways in exposed  $b$ - $c$  planes. A solid-solution reaction mechanism with  
6 small  $\text{Zn}^{2+}$  migration barrier and its derived intercalation pseudocapacitive behavior are also  
7 responsible for the fast electrochemical kinetics and rate capability. Full quasi-solid-state ZIBs  
8 assembled from such a ZOV array cathode and metallic Zn nanoflake array show high rate  
9 performance and long-cycle stability. No obvious aggregation, pulverization or dendrite growth  
10 has been observed on the Zn nanoflake array. Our encouraging results may boost further  
11 development of ZIBs by smart engineering of the array-type nanostructured electrode materials.  
12  
13  
14  
15  
16  
17  
18  
19  
20  
21  
22  
23  
24

### 25 Supporting Information

26 Supporting Information is available from the Wiley Online Library or from the author.  
27  
28

### 29 Acknowledgements

30 D.C. and C.Z. contributed equally to this work. This work is supported by the Singapore MOE AcRF  
31 Tier 1 grant (RG117/16, RG12/17) and Tier 2 grant (MOE2017-T2-1-073). M.S. thanks the Science  
32 Foundation of Jiangsu Province (BK20171169) and Jiangsu Higher Education Institutions  
33 (16KJB150037). H.Z. thanks the support from MOE under AcRF Tier 2 (MOE2014-T2-2-093,  
34 MOE2015-T2-2-057, and MOE2016-T2-2-103) and AcRF Tier 1 (2016-T1-001-147 and 2016-T1-002-  
35 051), and NTU under Start-Up Grant (M4081296.070.500000).  
36  
37  
38  
39  
40  
41  
42  
43  
44

### 45 References

- 46  
47 [1] J. F. Parker, C. N. Chervin, I. R. Pala, M. Machler, M. F. Burz, J. W. Long, D. R. Rolison, *Science* 2017, 356, 415.  
48 [2] H. Pan, Y. Shao, P. Yan, Y. Cheng, K. S. Han, Z. Nie, C. Wang, J. Yang, X. Li, P. Bhattacharya, K. T. Mueller, J. Liu,  
49 *Nature Energy* 2016, 1, 16039.  
50 [3] R. S. Carmichael, CRC Press, Boca Raton, FL 1988.  
51 [4] N. Zhang, F. Cheng, Y. Liu, Q. Zhao, K. Lei, C. Chen, X. Liu, J. Chen, *J. Am. Chem. Soc.* 2016, 138, 12894.  
52 [5] D. Kundu, B. D. Adams, V. D. Ort, S. H. Vajargah, L. F. Nazar, *Nature Energy* 2016, 1, 16119.  
53 [6] C. Xu, B. Li, H. Du, F. Kang, *Angewandte Chemie* 2012, 51, 933.  
54 [7] M. H. Alfaruqi, V. Mathew, J. Gim, S. Kim, J. Song, J. P. Baboo, S. H. Choi, J. Kim, *Chem. Mater.* 2015, 27, 3609.  
55 [8] L. Zhang, L. Chen, X. Zhou, Z. Liu, *Adv. Energy Mater.* 2015, 5, n/a.  
56 [9] G. Li, Z. Yang, Y. Jiang, C. Jin, W. Huang, X. Ding, Y. Huang, *Nano Energy* 2016, 25, 211.  
57  
58  
59  
60  
61  
62  
63  
64  
65

- [10] W. Li, K. Wang, S. Cheng, K. Jiang, *Energy Storage Mater.* 2018, 15, 14.
- [11] Q. Zhao, W. Huang, Z. Luo, L. Liu, Y. Lu, Y. Li, L. Li, J. Hu, H. Ma, J. Chen, *Science Advances* 2018, 4, eaao1761.
- [12] M. H. Alfaruqi, V. Mathew, J. Song, S. Kim, S. Islam, D. T. Pham, J. Jo, S. Kim, J. P. Baboo, Z. Xiu, K.-S. Lee, Y.-K. Sun, J. Kim, *Chem. Mater.* 2017, 29, 1684.
- [13] Y. Cai, F. Liu, Z. Luo, G. Fang, J. Zhou, A. Pan, S. Liang, *Energy Storage Mater.* 2018, 13, 168.
- [14] P. He, M. Yan, G. Zhang, R. Sun, L. Chen, Q. An, L. Mai, *Adv. Energy Mater.* 2017, 7, 1601920.
- [15] C. Xia, J. Guo, P. Li, X. Zhang, H. N. Alshareef, *Angewandte Chemie* 2018, 57, 3943.
- [16] J. Chmiola, G. Yushin, Y. Gogotsi, C. Portet, P. Simon, P. L. Taberna, *Science* 2006, 313, 1760.
- [17] D. Chao, C. Zhu, P. Yang, X. Xia, J. Liu, J. Wang, X. Fan, S. V. Saviolov, J. Lin, H. J. Fan, Z. X. Shen, *Nat. Commun.* 2016, 7, 12122.
- [18] D. Chao, P. Liang, Z. Chen, L. Bai, H. Shen, X. Liu, X. Xia, Y. Zhao, S. V. Saviolov, J. Lin, Z. X. Shen, *ACS Nano* 2016, 10, 10211; Y. Huang, W. S. Ip, Y. Y. Lau, J. Sun, J. Zeng, N. S. S. Yeung, W. S. Ng, H. Li, Z. Pei, Q. Xue, Y. Wang, J. Yu, H. Hu, C. Zhi, *ACS Nano* 2017, 11, 8953.
- [19] X. Wang, F. Wang, L. Wang, M. Li, Y. Wang, B. Chen, Y. Zhu, L. Fu, L. Zha, L. Zhang, Y. Wu, W. Huang, *Adv. Mater.* 2016, 28, 4904.
- [20] D. Chao, C. Zhu, X. Xia, J. Liu, X. Zhang, J. Wang, P. Liang, J. Lin, H. Zhang, Z. X. Shen, H. J. Fan, *Nano Lett.* 2015, 15, 565.
- [21] D. Chao, X. Xia, J. Liu, Z. Fan, C. F. Ng, J. Lin, H. Zhang, Z. X. Shen, H. J. Fan, *Adv. Mater.* 2014, 26, 5794.
- [22] B. Pal, D. Chakravorty, *The Journal of Physical Chemistry B* 2006, 110, 20917.
- [23] J. F. Parker, E. S. Nelson, M. D. Wattendorf, C. N. Chervin, J. W. Long, D. R. Rolison, *ACS Appl. Mater. Interfaces* 2014, 6, 19471.
- [24] B. Li, Z. Nie, M. Vijayakumar, G. Li, J. Liu, V. Sprenkle, W. Wang, *Nat. Commun.* 2015, 6, ncomms7303.
- [25] M. Yan, P. He, Y. Chen, S. Wang, Q. Wei, K. Zhao, X. Xu, Q. An, Y. Shuang, Y. Shao, K. T. Mueller, L. Mai, J. Liu, J. Yang, *Adv. Mater.* 2018, 30; Y. Zeng, X. Zhang, Y. Meng, M. Yu, J. Yi, Y. Wu, X. Lu, Y. Tong, *Adv. Mater.* 2017, 29.
- [26] C. Xia, J. Guo, Y. Lei, H. Liang, C. Zhao, H. N. Alshareef, *Adv. Mater.* 2018, 30.
- [27] M. Yan, F. Wang, C. Han, X. Ma, X. Xu, Q. An, L. Xu, C. Niu, Y. Zhao, X. Tian, P. Hu, H. Wu, L. Mai, *J. Am. Chem. Soc.* 2013, 135, 18176; X. Lu, M. Yu, G. Wang, Y. Tong, Y. Li, *Energy Environ. Sci.* 2014, 7.
- [28] L. Suo, O. Borodin, W. Sun, X. Fan, C. Yang, F. Wang, T. Gao, Z. Ma, M. Schroeder, A. v. Cresce, S. M. Russell, M. Armand, A. Angell, K. Xu, C. Wang, *Angew. Chem. Int. Ed.* 2016, 55, 7136.
- [29] D. Su, A. McDonagh, S. Z. Qiao, G. Wang, *Adv. Mater.* 2016, 29.
- [30] N. Wang, Z. Bai, Y. Qian, J. Yang, *Adv. Mater.* 2016, 28, 4126.
- [31] C. Guan, W. Zhao, Y. Hu, Q. Ke, X. Li, H. Zhang, J. Wang, *Adv. Energy Mater.* 2016, 6.
- [32] Y. Zeng, Z. Lin, Y. Meng, Y. Wang, M. Yu, X. Lu, Y. Tong, *Adv. Mater.* 2016, 28, 9188.
- [33] L. Li, S. Peng, H. B. Wu, L. Yu, S. Madhavi, X. W. D. Lou, *Adv. Energy Mater.* 2015, n/a.
- [34] Z. Chen, V. Augustyn, X. Jia, Q. Xiao, B. Dunn, Y. Lu, *ACS Nano* 2012, 6, 4319.
- [35] X. Wang, S. Kajiyama, H. Iinuma, E. Hosono, S. Oro, I. Moriguchi, M. Okubo, A. Yamada, *Nat. Commun.* 2015, 6, 6544.
- [36] H. Kim, M.-Y. Cho, M.-H. Kim, K.-Y. Park, H. Gwon, Y. Lee, K. C. Roh, K. Kang, *Adv. Energy Mater.* 2013, 3, 1500.
- [37] J. Come, V. Augustyn, J. W. Kim, P. Rozier, P. L. Taberna, P. Gogotsi, J. W. Long, B. Dunn, P. Simon, *J. Electrochem. Soc.* 2014, 161, A718.
- [38] E. Hryha, E. Rutqvist, L. Nyborg, *Surf. Interface Anal.* 2012, 44, 1022.
- [39] R. Tripathi, S. M. Wood, M. S. Islam, L. F. Nazar, *Energy Environ. Sci.* 2013, 6, 2257; M. S. Islam, D. J. Driscoll, C. A. J. Fisher, P. R. Slater, *Chem. Mater.* 2005, 17, 5085; A. Emly, A. Van der Ven, *Inorg. Chem.* 2015, 54, 4394; X. Zhao, X. Zhang, D. Wu, H. Zhang, F. Ding, Z. Zhou, *J. Mater. Chem. A* 2016, 4, 16606; Vadym V. Kulish, S. Manzhos,

RSC Adv. 2017, 7, 18643; P. Barpanda, G. Oyama, S. Nishimura, S. C. Chung, A. Yamada, Nat. Commun. 2014, 5, 4358.

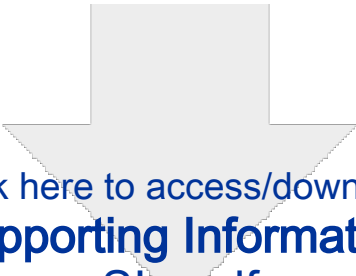
[40] V. Augustyn, J. Come, M. A. Lowe, J. W. Kim, P. L. Taberna, S. H. Tolbert, H. D. Abruña, P. Simon, B. Dunn, Nat. Mater. 2013, 12, 518.

[41] G. A. Muller, J. B. Cook, H. S. Kim, S. H. Tolbert, B. Dunn, Nano Lett. 2015, 15, 1911.

[42] T. Brezesinski, J. Wang, S. H. Tolbert, B. Dunn, Nat. Mater. 2010, 9, 146.

[43] J. Wang, J. Polleux, J. Lim, B. Dunn, J. Phys. Chem. C 2007, 111, 14925.

[44] D. Chao, C.-H. M. Lai, P. Liang, Q. Wei, Y.-S. Wang, C. R. Zhu, G. Deng, V. V. T. Doan-Nguyen, J. Lin, L. Mai, H. J. Fan, B. Dunn, Z. X. Shen, Adv. Energy Mater. 2018, 10.1002/aenm.201800058.



Click here to access/download  
**Supporting Information**  
SI-r.pdf

